Enhancement of Tropical Ocean Evaporation and Sensible Heat Flux by Atmospheric Mesoscale Systems

Steven K. Esbensen

College of Oceanic and Atmospheric Sciences, Oregon State University, Corvallis, Oregon

Michael J. McPhaden

NOAA/Pacific Marine Environmental Laboratory, Seattle, Washington

(Manuscript received 18 September 1995, in final form 12 April 1996)

ABSTRACT

The enhancement of monthly averaged evaporation by atmospheric mesoscale systems is estimated from long-term hourly observations of surface meteorological data from the Tropical Ocean Global Atmosphere (TOGA) Tropical Atmosphere Ocean (TAO) buoy moorings over the equatorial Pacific Ocean and a bulk aerodynamic flux algorithm developed as a result of the TOGA Coupled Ocean–Atmosphere Response Experiment (COARE). It is shown that mesoscale enhancement is due primarily to the lack of wind steadiness on subsynoptic timescales and is associated with periods of significant precipitation.

The magnitude of the mesoscale enhancement of monthly averaged sea surface evaporation is found to be ~10% or less of the total. During occasional periods with weak and variable winds over the western Pacific warm pool and the other major precipitation zones in the equatorial Pacific, the mesoscale enhancement of monthly averaged evaporation can reach 30% of the total evaporation.

A similar result is obtained for mesoscale enhancement of diffusive air–sea sensible heat transfer using data from TOGA TAO moorings. However, a comparison of results from the colocated TAO and Improved METeo-rological measurements (IMET) moorings during TOGA COARE, and results previously reported from a pre-COARE cruise in the western Pacific warm pool region, indicate that processes in addition to mesoscale wind variability may be important contributors to the mesoscale enhancement of the sensible heat flux.

It is suggested that the most important effects of atmospheric mesoscale systems on tropical ocean evaporation and sensible heat flux are represented in existing climatologies.

1. Introduction

It is well established that monthly averaged wind speeds, temperatures, and humidities may be used to estimate the monthly averaged open ocean surface evaporation[1] and sensible heat flux from the bulk aerodynamic equations with a relative error of ~10% or less, except where the bulk aerodynamic estimates are near zero and the relative error does not provide a useful measure of accuracy. The use of monthly averaged meteorological data for flux calculations has been referred to as the classical method by Esbensen and Reynolds (1981), in contrast to the sampling method, which computes the sample monthly mean from indi-

vidual bulk aerodynamic flux estimates. The accuracy of the classical method has been estimated for the mid-latitude and subtropical oceans by Esbensen and Reynolds (1981) and Josey et al. (1995) using ocean weather ship data, and by Gulev (1994) for a region southeast of Newfoundland using a variety of in situ surface meteorological measurements. The classical method accuracy has also been examined for the equatorial oceans by Liu (1988) and Zhang (1995) using data from moored buoys. Most global climatological computations to date have used the classical method (Budyko 1963; Esbensen and Kushnir 1981; Hsuing 1986; Oberhuber 1988), although a Comprehensive Ocean–Atmosphere Data Set (COADS) analysis using the sampling method has been published recently (da Silva et al. 1994).

The classical method for computing evaporation and sensible heat flux works as well as it does in middle and subtropical latitudes primarily because it uses the monthly average of the scalar wind speed, rather than the speed computed from the monthly average of the vector wind components. A secondary reason for the success of the classical method is the fortuitous can-

---

[1] The terms evaporation and latent heat flux will be used interchangeably in this tropical study.

Corresponding author address: Prof. S. K. Esbensen, College of Oceanic and Atmospheric Sciences, Oregon State University, Corvallis OR 97331-2209.
E-mail: esbensen@ats.orst.edu

cellation of some nonlinear terms involving correlations of the transfer coefficient with wind speed and the air–sea temperature and humidity differences (Esbensen and Reynolds 1981; Josey et al. 1995). In comparison with conditions over land (e.g., Mahrt et al. 1986; Sun and Mahrt 1995), the stability of the marine surface boundary layer tends to be relatively constant in space and time throughout the day. The nonlinearities introduced through diurnal variation of the transfer coefficients are not strong enough to cause large errors in classical method estimates in midlatitude and subtropical ocean regimes. Furthermore, the flux due to the covariance between variations in the wind speed and the air–sea temperature and humidity differences is no more than 10% of the monthly averaged flux over most of the global oceans, even in wintertime midlatitude storm tracks. The reader is referred to Esbensen and Reynolds (1981) and Josey et al. (1995) for further discussion.

In the oceanic Tropics, synoptic-scale disturbances are typically not associated with strong horizontal advection of temperature and moisture. The vertical movement of air in convective cloud systems provides the primary mechanism for rapid changes of boundary layer thermodynamic properties. Case studies have consistently shown that the sensible heat flux in the wakes of mesoscale convective systems can be an order of magnitude larger than the undisturbed boundary layer air in the surroundings (e.g., Johnson and Nicholls 1983; Young et al. 1992). Johnson and Nicholls (1983) find a fourfold enhancement of evaporation associated with a steady moving squall line in the northeastern Atlantic intertropical convergence zone (ITCZ). Evaporation enhancements in the western Pacific warm pool region have been observed to be smaller and less systematic (Young et al. 1992).

If we are to believe existing climatologies of evaporation (e.g., Esbensen and Kushnir 1981; Oberhuber 1988), however, the regions of deep convection and rainfall over the tropical oceans are not maxima in the evaporation fields. One cannot clearly identify the regions of heavy tropical precipitation from an inspection of climatological evaporation fields. In fact, the climatologies show that the equatorial zone has generally lower values of evaporation than the tradewind zones to the north and south. The sensible heat flux field is also relatively broad and featureless in regions of deep tropical convection, although uncertainties involved in measuring the small air–sea temperature from voluntary observing ships (e.g., Kent et al. 1993) make a definite conclusion impossible at this point.

We therefore pose the following questions: How large is the enhancement of monthly averaged evaporation and sensible heat flux by atmospheric mesoscale systems and is it possible that existing climatologies have missed a large enhancement of evaporation by tropical convective systems through inadequate sampling of the boundary layer in tropical mesoscale cloud systems? The potential importance of such evaporation enhancements for climate modeling has been demonstrated in the sensitivity study by Miller et al. (1992). The objective of this study is to provide a quantitative climatological estimate of the magnitude of the mesoscale enhancement over the tropical Pacific Ocean.

Using the unprecedented dataset from the Tropical Ocean Global Atmosphere (TOGA) Tropical Atmosphere Ocean (TAO) array of moored buoys over the equatorial Pacific, and IMET data from the TOGA Coupled Ocean–Atmosphere Response Experiment (COARE), we will estimate the enhancement of evaporation and sensible heat flux by mesoscale convective systems. We will see that large local enhancements of evaporation and sensible heat flux can occur on a given day during a month with significant precipitation, but that the large flux enhancement events apparently do not occur with sufficient frequency or duration to have a dramatic effect on the monthly averaged total evaporation and sensible heat flux fields.

We will find that the magnitude of the mesoscale enhancement of monthly averaged sea surface evaporation and diffusive sensible heat transfer to the atmosphere is $\sim$10% or less of the total. During occasional periods with weak and variable winds over the western Pacific warm pool and the other major precipitation zones in the equatorial Pacific, the mesoscale enhancement of monthly averaged evaporation fields can reach 30% of the total evaporation. These findings are consistent with the Ledvina et al. (1993) analysis of evaporation and sensible heat flux estimates using boundary layer data from a three-week pre-COARE cruise in the western Pacific warm pool region, and extend the analysis to the entire equatorial Pacific for all months of the year. Our results suggest that existing climatologies contain most of the total signal for tropical evaporation and sensible heat flux, but that accounting for the mesoscale enhancement of evaporation and sensible heat flux may be required for understanding and modeling the disturbances whenever spatial or temporal differences $\sim$10 W m^{-2} are important for the evolution of a specific large-scale tropical disturbance.

Section 2 presents the methodology for estimating mesoscale enhancements of evaporation and sensible heat flux, which is followed in section 3 by a brief description of the TAO and Improved METeorological Measurements (IMET) buoy datasets. Results are presented and discussed in sections 4 and 5.

2. Methodology

The central working hypothesis of this study is that it is possible to isolate and measure mesoscale enhancements of large-scale surface evaporation and sensible heat flux through the use of simple temporal averages of moored buoy time series. It will be assumed that the bulk aerodynamic formulas are adequate to describe the local relationship between the surface fluxes and bulk

TABLE 1. Analyzed TAO buoy locations.

143°E	147°E	156°E	158°E	165°E
				8°N
	5°N	5°N		5°N
	2°N	2°N		2°N
EQ		EQ	EQ	EQ
		2°S		2°S
				8°S

180°W	170°W	155°W	140°W	125°W	110°W	95°W
			9°N			
	8°N			8°N	8°N	
5°N	5°N	5°N		5°N	5°N	
2°N	2°N	2°N		2°N	2°N	2°N
EQ	EQ	EQ	EQ	EQ	EQ	
2°S	2°S		2°S	2°S	2°S	2°S
5°S	5°S	5°S	5°S	5°S	5°S	
	8°S	8°S			8°S	

wind, temperature, and humidity variables. The problem of analyzing the mesoscale enhancement of the surface fluxes then becomes one of describing the co-variability of the bulk properties in time. The results of the time series analysis may then be used to evaluate the possible importance of mesoscale systems in determining the climatological fields of evaporation and sensible heat in key climatic regimes over the tropical oceans.

a. The bulk aerodynamic method

We assume that the surface evaporation E and diffusive sensible heat flux S may be estimated from bulk aerodynamic formulas relating the turbulent flux of water vapor and sensible heat just above the sea surface to locally averaged values of sea surface temperature, and wind speed, air temperature, and humidity in the surface boundary layer. The bulk aerodynamic formulas may be written

$$E = \overline{\rho w' q'}$$
$$= \overline{\rho} C_q(\cdots, z_u, z_q) U(z_u) [\overline{q}_{sfc} - \overline{q}(z_q)] \quad (1)$$

$$S = \overline{\rho}\, \overline{c_p w' T'}$$
$$= \overline{\rho}\, \overline{c_p} C_\theta(\cdots, z_u, z_\theta) U(z_u) [\overline{\theta}_{sfc} - \overline{\theta}(z_\theta)], \quad (2)$$

where ρ and c_p are the air density and specific heat at constant pressure, respectively, and $C_q(\ldots, z_u, z_q)$ and $C_\theta(\ldots, z_u, z_\theta)$ are the transfer coefficients defined in terms of the specific humidity q and the potential temperature θ, respectively. The transfer coefficients C_q and C_θ depend on sea state, atmospheric surface boundary layer stability, and the observation heights z_u, z_q, and z_θ above the surface. Overbars indicate a local time averaging operator that defines the turbulent fluctuations; fluctuations are denoted by primes, for example, $q' = q - \overline{q}$. The local averaging scale is chosen in such

a way that it separates variability due to turbulence and convection from mesoscale and synoptic-scale variability. Mahrt and Sun (1995) and Sun et al. (1996) discuss the dependence of E and S on the choice of the local averaging length scale. The quantity $U(z_u) [\equiv (\overline{u}^2 + \overline{v}^2)^{1/2}]$ is the wind speed calculated from a local average of the vector wind components[2] at height z_u, while $\overline{q}_{sfc}$, $\overline{\theta}_{sfc}$, $\overline{q}(z_q)$, and $\overline{\theta}(z_\theta)$ are the locally averaged values of specific humidity and potential temperature at the sea surface and heights z_q and z_θ, respectively.

We adopt the COARE (version 2.0) algorithm (Fairall et al. 1996b) for evaluating E and S from the bulk aerodynamic formulas. The COARE algorithm recalibrates and extends the Liu–Katsaros–Businger formulation (Liu et al. 1979) using turbulence data from TOGA COARE. The new algorithm includes a separate model that permits the determination of the ocean skin temperature from buoy observations of subsurface temperature, provided that the time history of incoming atmospheric radiation is known.

We have made several minor modifications to the COARE algorithm for the purposes of this study. To be consistent with the conventional definition of the bulk aerodynamic formulas in Eqs. (1) and (2), we absorb the gustiness parameter dependence (see Fairall et al. 1996b) into our definition of the transfer coefficient. For simplicity, we assume ρ, c_p, and the latent heat of vaporization L are constant and equal to 1.2 kg m^{-3}, 1005 J kg^{-1} K^{-1}, and 2.5 × 10^6 J kg^{-1}, respectively. In other words we do not consider the so-called Webb correction to evaporation or the small difference between S evaluated by $\overline{\rho}\,c_p w' T'$ and the true thermal conduction of heat at the sea surface, which involves the so-called moisture correction term to the sensible heat flux; discussions of these effects can be found in Businger (1982) and Sun et al. (1995). The constant value of L is used whenever it is needed to convert between evaporation and latent heat flux. A slightly more accurate saturation vapor pressure routine is used for all of our calculations (Buck 1981).

b. Definition of mesoscale enhancement

Data from the TAO and IMET buoys may be regarded as regularly spaced time series consisting of locally averaged field variables at a fixed point in space. Let us define a large-scale averaging operator of the form

$$\langle (\ ) \rangle = \frac{1}{N} \sum_{n=1}^{N} (\ )_n \quad (3)$$

that separates the signal into its synoptic-scale and smaller-scale parts. Here n is the time index and N is a

---

[2] To be more accurate, u and v should be evaluated as the velocity shear between the wind at z_u and the ocean surface current.

TAO Mooring 9N140W
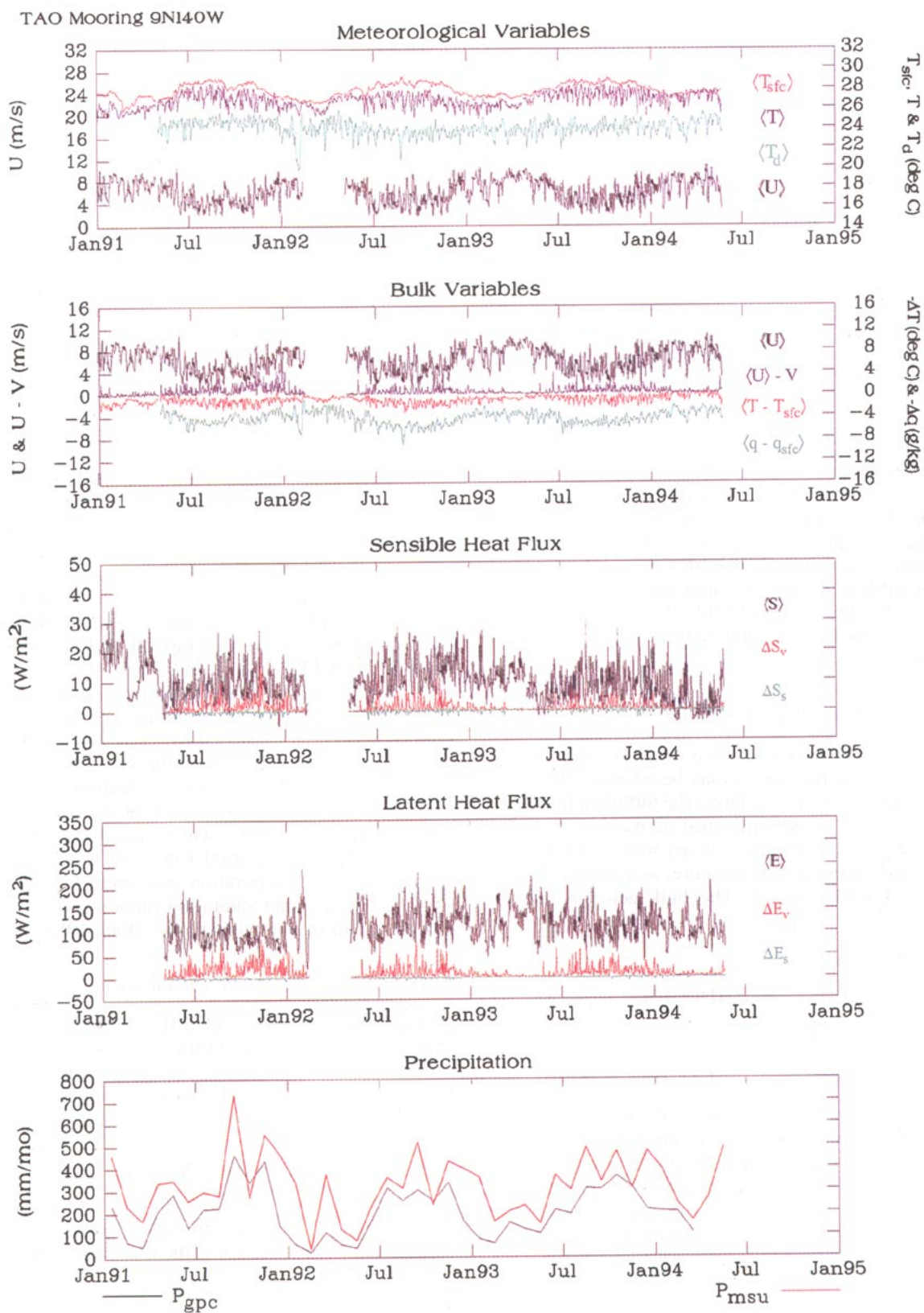
constant corresponding to the period of the uniformly weighted time average.

We may use the averaging operator in Eq. (3) to define three measures of ocean surface evaporation and sensible heat flux.

Total flux

$$\langle E \rangle = \rho \langle C_q U(q_{sfc} - q) \rangle \tag{4}$$

$$\langle S \rangle = \rho c_p \langle C_\theta U(\theta_{sfc} - \theta) \rangle. \tag{5}$$

Scalar-mean flux

$$E_s = \rho C_q(\langle U \rangle, \langle \cdot \rangle) \langle U \rangle (\langle q_{sfc} \rangle - \langle q \rangle) \tag{6}$$

$$S_s = \rho c_p C_\theta(\langle U \rangle, \langle \cdot \rangle) \langle U \rangle (\langle \theta_{sfc} \rangle - \langle \theta \rangle). \tag{7}$$

Vector-mean flux

$$E_v = \rho C_q(V, \langle \cdot \rangle) V (\langle q_{sfc} \rangle - \langle q \rangle) \tag{8}$$

$$S_v = \rho c_p C_\theta(V, \langle \cdot \rangle) V (\langle \theta_{sfc} \rangle - \langle \theta \rangle). \tag{9}$$

In Eqs. (4)–(9), we have dropped the averaging operator symbols on ρ and c_p since we have assumed them to be constants. We have also dropped the local averaging operator denoted by overbars on the wind and thermodynamic variables without ambiguity. The vector averaged wind, V, is defined as the wind speed computed from the large-scale average of the vector wind components; that is, $V \equiv (\langle u \rangle^2 + \langle v \rangle^2)^{1/2}$. The transfer coefficients for E_s and S_s are obtained by formally substituting $\langle U \rangle$ and time-averaged thermodynamic variables indicated by $\langle \cdot \rangle$ into the transfer coefficient algorithm. The transfer coefficients for E_v and S_v are determined in an identical manner to the scalar-mean flux, except that V is formally substituted for the wind speed.

We define mesoscale enhancement of evaporation and sensible heat flux as $\Delta E \equiv \langle E \rangle - E_v$ and $\Delta S \equiv \langle S \rangle - S_v$, respectively. The vector mean fluxes E_v and S_v represent the air–sea flux estimates that would be computed by formal substitution of synoptic-scale fields of sea surface temperature, vector wind speed, and thermodynamic variables into the bulk aerodynamic formulas. If mesoscale disturbances were nonexistent, we would expect the large-scale flux to equal the vector-averaged flux and the mesoscale enhancement to be zero. In general, mesoscale disturbances may modulate the surface fluxes through nonlinear interactions of wind and thermodynamic fields, creating a discrepancy between the total flux and the vector-averaged flux.

TABLE 2. Root-mean-square flux errors due to TAO temporal sampling strategy.

	2°S,156°E	EQ,165°E	EQ,110°W(1)	EQ,110°W(2)
(a) Hourly estimates: Sensible heat flux				
Mean flux	12.2	5.8	2.4	0.9
Std dev	12.6	3.8	4.9	3.8
Rms diff	3.30	0.77	0.45	0.49
Rms diff/std	0.26	0.20	0.09	0.13
No. estimates	3193	2927	4304	4364
(b) Daily estimates: Sensible heat flux				
Mean flux	12.2	5.8	2.4	0.9
Std dev	7.9	2.4	4.2	3.3
Rms diff	0.46	0.13	0.08	0.06
Rms diff/std	0.06	0.05	0.02	0.02
No. estimates	132	121	178	182

	2°S,156°E
(c) Hourly estimates: Latent heat flux	
Mean flux	131.5
Std dev	56.7
Rms diff	19.95
Rms diff/std	0.35
No. estimates	3193
(d) Daily estimates: Latent heat flux	
Mean flux	131.4
Std dev	43.4
Rms diff	2.82
Rms diff/std	0.06
No. estimates	132

This discrepancy is our measure of mesoscale enhancement.

To isolate the effect of wind variability, we further decompose the mesoscale enhancement of evaporation ΔE and sensible heat flux ΔS into two parts,

$$\Delta E \equiv \langle E \rangle - E_v = \Delta_s E + \Delta_v E \tag{10}$$

$$\Delta S \equiv \langle S \rangle - S_v = \Delta_s S + \Delta_v S, \tag{11}$$

where $\Delta_s E \equiv \langle E \rangle - E_s$, $\Delta_v E \equiv E_s - E_v$, $\Delta_s S \equiv \langle S \rangle - S_s$ and $\Delta_v S \equiv S_s - S_v$. The quantities $\Delta_s E$ and $\Delta_s S$ correspond to the differences between the classical and sampling methods discussed in the introduction, except we are dealing with a time average on the order of a day, rather than a monthly average. The quantities $\Delta_v E$ and $\Delta_v S$ measure the portion of the mesoscale enhance-

FIG. 1. (a) Time series of daily averaged 1-m water temperature, air temperature, dewpoint, and scalar-averaged wind speed at the 9°N, 140°W TAO mooring. (b) Time series of the daily averaged scalar average wind speed $\langle U \rangle$, the difference between the scalar average and vector average wind speed $\langle U \rangle - V$, the air-minus-water temperature difference, and the air-minus-"surface" specific humidity difference at the 9°N, 140°W TAO mooring. The 1-m water temperature is used for T_{sfc}, and to calculate q_{sfc}. (c) and (d) Time series of daily averaged sensible heat flux and latent heat flux estimates and their enhancement by atmospheric mesoscale systems at the 9°N, 140°W TAO mooring. See section 2b for definition of mesoscale enhancement. (e) Time series of monthly averaged GOES Precipitation Index (dashed line) and Microwave Sounding Unit (solid line) precipitation estimates are presented as a measure of convective activity.

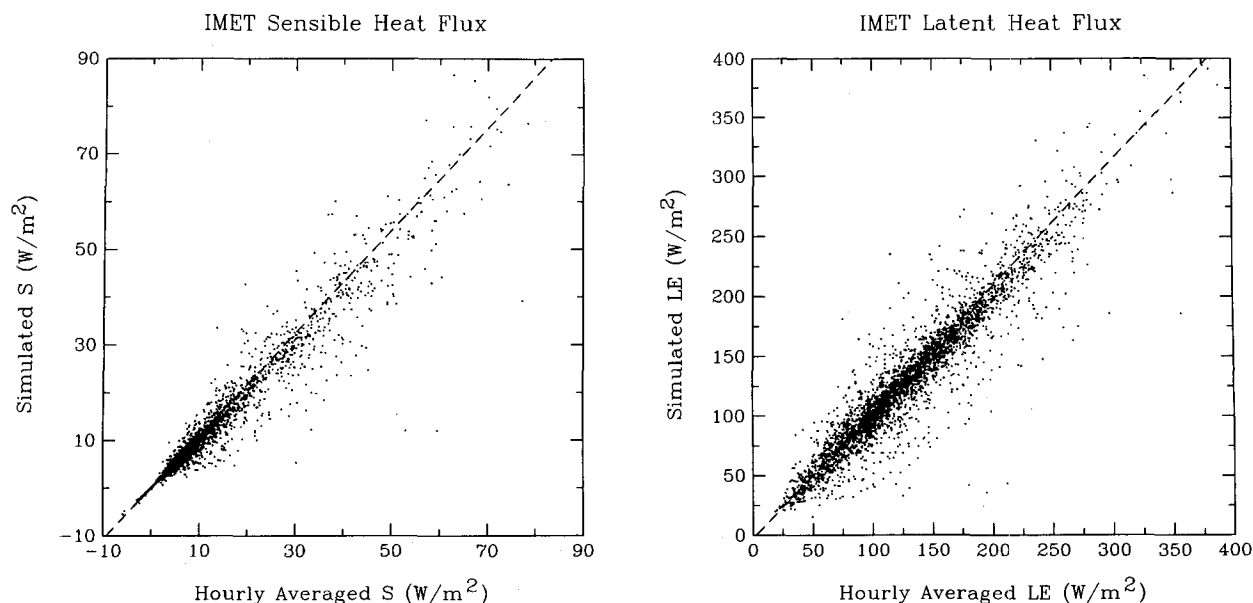IMET Sensible Heat Flux   IMET Latent Heat Flux

FIG. 2. Simulated temporal sampling errors of TAO moorings for estimates of the hourly averaged sensible and latent heat fluxes. The scatterplot compares hourly averaged flux values at the TOGA COARE IMET mooring with hourly averaged flux values obtained by applying the TAO sampling pattern to the IMET data. See section 3 for details.

ment of evaporation and sensible heat flux that can be explained by mesoscale wind variations alone. It should be noted that if there were no variation in wind direction, then $\langle U \rangle$ would equal V and $\Delta_v E$ and $\Delta_v S$ would be zero.

c. Selection of averaging scale

The above definition of mesoscale enhancement requires the selection of an averaging timescale that separates mesoscale convective systems from their synoptic-scale environment. Since tropical mesoscale convective systems have typical lifetimes of ~ 10 h (Houze 1993), we choose 24 h as as the large-scale averaging period.

TABLE 3. Statistics of mesoscale enhancement of sensible and latent heat fluxes at 9°N 140°W TAO mooring during the rainy half of the year, the "ITCZ regime," from 1 July to 31 December during the years 1991–1994.

	Mean (W m^{-2})	Std dev (W m^{-2})	Skewness	Percent mean × 100
$L\langle E \rangle$	113.3	33.1	0.65	100
$L\Delta E_s$	−1.3	1.7	−1.44	−1
$L\Delta E_v$	16.5	15.3	1.56	15
$L\Delta E$	15.2	15.0	1.59	13
$\langle S \rangle$	10.7	6.2	0.65	100
ΔS_s	−0.1	0.6	−0.55	−1
ΔS_v	1.8	2.3	2.73	17
ΔS	1.7	2.3	2.27	16

In nature, there is no clear separation between synoptic and mesoscale systems. Furthermore, our method does not distinguish between diurnal variation of large-scale fields and the signals directly attributable to mesoscale convective systems. The values of mesoscale enhancement estimated from the buoy analysis will therefore suffer from some ambiguity in terms of scale separation and the mixing of synoptic-scale diurnal variability with the signal from mesoscale convective systems. We do not believe that this is a serious deficiency. It might also be argued that individual elements of convective systems having shorter timescales, such as individual convective cells at the leading edge of banded mesoscale systems, should not be included in the definition of mesoscale enhancement. These elements, however, are characteristic features of mesoscale convective systems. We would therefore argue that the contributions to the total flux by smaller-scale elements of the convective systems should be regarded as part of mesoscale enhancement for the purposes of this discussion.

d. Sampling error

For a given mesoscale convective system, a moored buoy may sample only a portion of the system as it evolves in space and time. Over the period of a month in a convectively active region, however, we expect that a moored buoy will sample a significant number of systems in all stages of development. In the absence of strong mesoscale sea surface temperature gradients that might preferentially trigger convective systems at

TAO Mooring 9N140W

Sensible Heat Flux

Latent Heat Flux

Precipitation

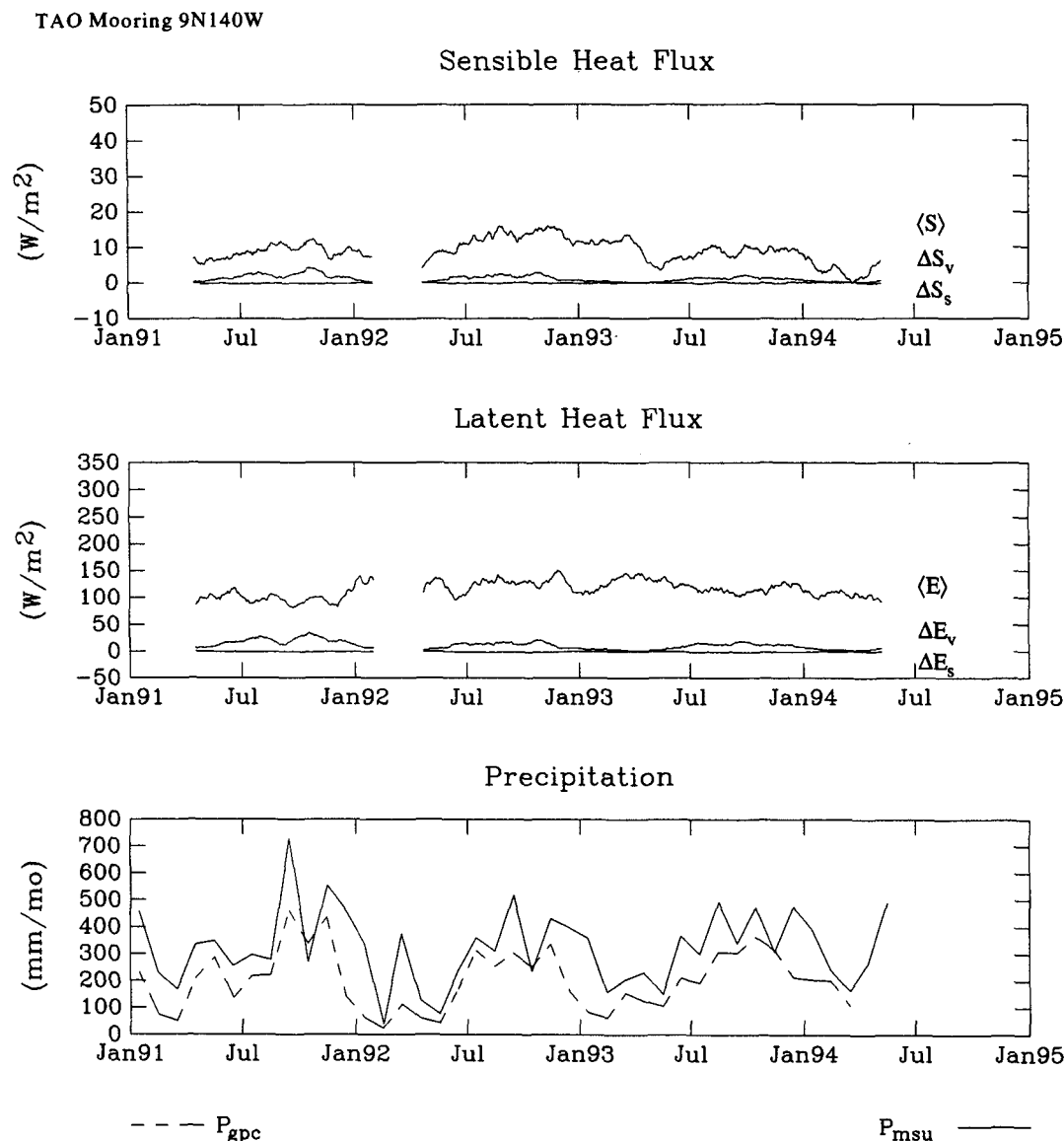$- - - \mathrm{P_{gpc}}$　　　　　　　　　　$\mathrm{P_{msu}}$ ———

FIG. 3. Thirty-day running mean of daily averaged sensible heat flux and latent heat flux estimates and their enhancement by atmospheric mesoscale systems at the 9°N, 140°W TAO mooring. See section 2b for definition of mesoscale enhancement. Time series of monthly averaged GOES Precipitation Index (dashed line) and Microwave Sounding Unit (solid line) precipitation estimates are presented as a measure of convective activity.

a particular spatial location, we expect that the evaporation and sensible heat flux statistics measured at two nearby buoy locations separated by a distance ~10 km would not differ in a qualitative sense over the period of a month. Analysis of data from two colocated TOGA COARE moorings (see section 4c) will support this assertion.

3. Datasets

a. TOGA TAO moored buoy array

The Tropical Atmosphere Ocean (TAO) buoy array consists of 69 moored buoys deployed in a regular ar-

ray across the equatorial Pacific Ocean as part of the Tropical Ocean Global Atmosphere Program (Hayes et al. 1991; McPhaden 1995). For this study, we have extracted and analyzed all records having at least one month of continuous hourly observations through the end of 1994 and having simultaneous reports of the vector wind (u, v), sea surface temperature T_{sfc}, air temperature T, and relative humidity RH. A list of the buoy time series satisfying our criteria is given in Table 1. In addition to the extensive quality control and data editing performed by the NOAA Pacific Marine Environmental Laboratory, a very small number of the re-

TAO Mooring 2N147E

Sensible Heat Flux
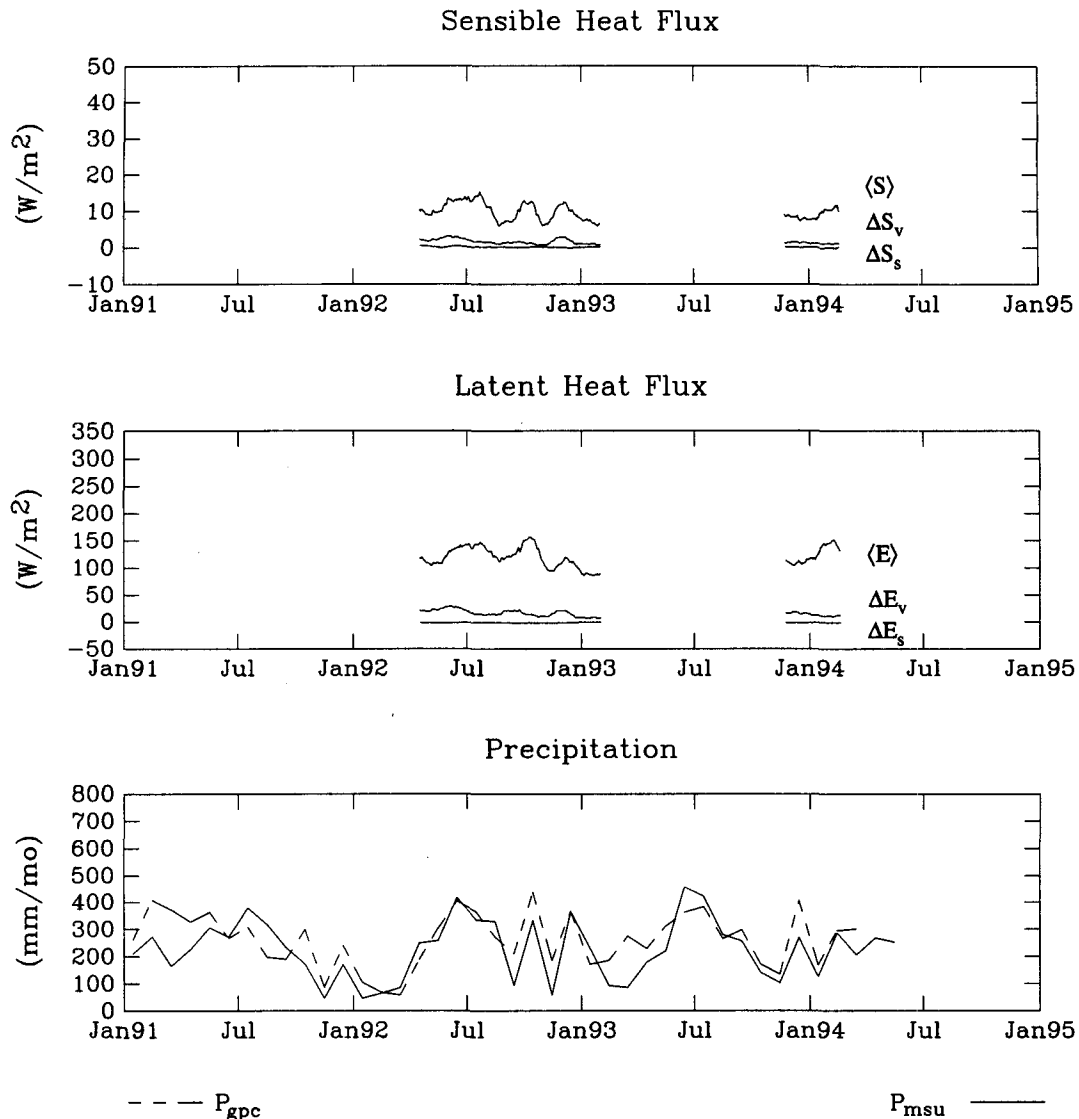

Latent Heat Flux

Precipitation

FIG. 4. As in Fig. 3 except for the 2°N, 147°E TAO mooring.

maining data points and records having obvious data quality problems have been removed from the analysis.

The reliability of the TAO system is remarkable for an untended system at sea. Figure 1a shows daily averaged meteorological variables computed from the hourly observations at the 9°N, 140°W mooring; a daily averaged value was not computed if any of the 24 hourly reports was missing. For more than a year, the buoy system returned an essentially countinuous time series of hourly values having no obvious data quality problems. The existence of such long records makes it possible to examine a wide range of disturbed and undisturbed boundary layer conditions using a uniformly sampled time series.

The reported hourly values of T_{sfc}, T, and RH are the arithmetic average of six evenly spaced samples throughout the hour. The reported wind vector is a 6-min average of the vector wind components from digital 2-Hz samples at the top of the hour. A 6-min average is a reasonable length of time to integrate over the turbulent elements carrying most of the flux. For example, a mean 3 m s^{-1} wind would advect ~1.1 km of air past the buoy, which, using Taylor's hypothesis, would be sufficient to relate turbulent flux to bulk parameters in the equatorial zone (Sun et al. 1996).

In principle, the local average designated by the overbar in Eqs. (1) and (2) should be applied consistently to all wind and thermodynamic data. The

TAO Mooring 2S110W

Sensible Heat Flux

Latent Heat Flux

Precipitation

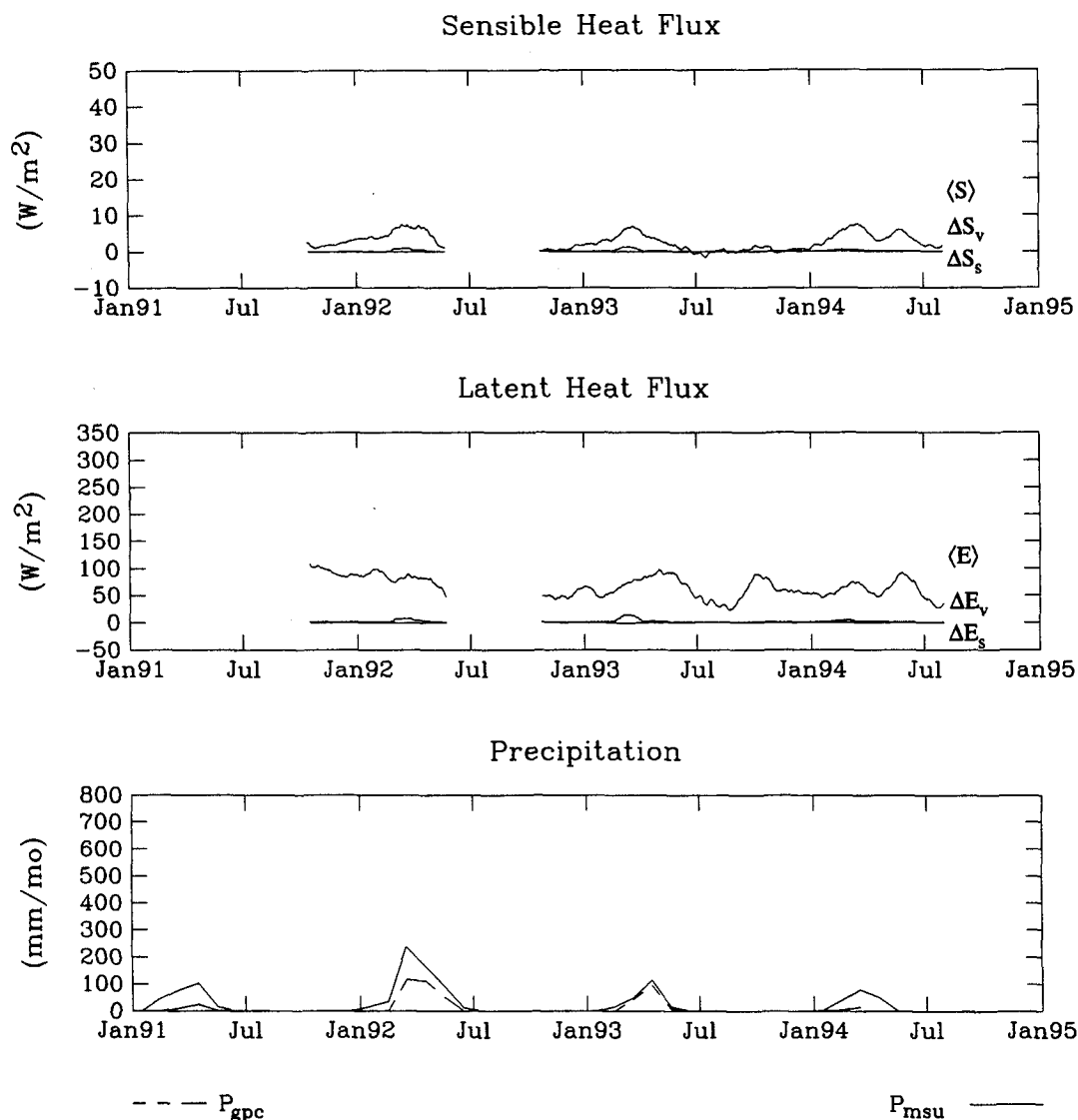$- - - \ P_{gpc}$　　　　　　　　　　　P_{msu} ————

FIG. 5. As in Fig. 3 except for the 2°S, 110°W TAO mooring.

TAO sampling strategy, however, was not designed for turbulent flux estimates, but was driven by mean wind and temperature sampling requirements plus engineering requirements (e.g., power consumption). The present sampling strategy is therefore a compromise.[3] We have examined the effect of the sampling strategy on bulk aerodynamic flux estimates by simulating TAO buoy data using independent data from an older style TAO mooring reporting 15-min averages, and by using the TOGA COARE

IMET mooring at 2°S, 156°E reporting 7.5-min averages for all bulk variables from 21 October 1992 through 3 March 1993. The TAO moorings were located at EQ, 165°E during 24 December 1988 through 24 April 1989, and at EQ, 110°W during 1 May through 27 October 1987 (period 1) and from 1 November 1987 through 30 April 1988. The simulation results are shown in Table 2 and are illustrated in Fig. 2. At the IMET mooring, the rms errors introduced by the sampling strategy are 3 W m^{-2} for the hourly averaged sensible heat flux and 20 W m^{-2} for the hourly averaged latent heat flux. The fluxes computed with sampled data from the simulated TAO data are highly correlated with properly com-

---

[3] The next generation of ATLAS moorings to be used in the TAO array will better synchronize the sampling of all variables.

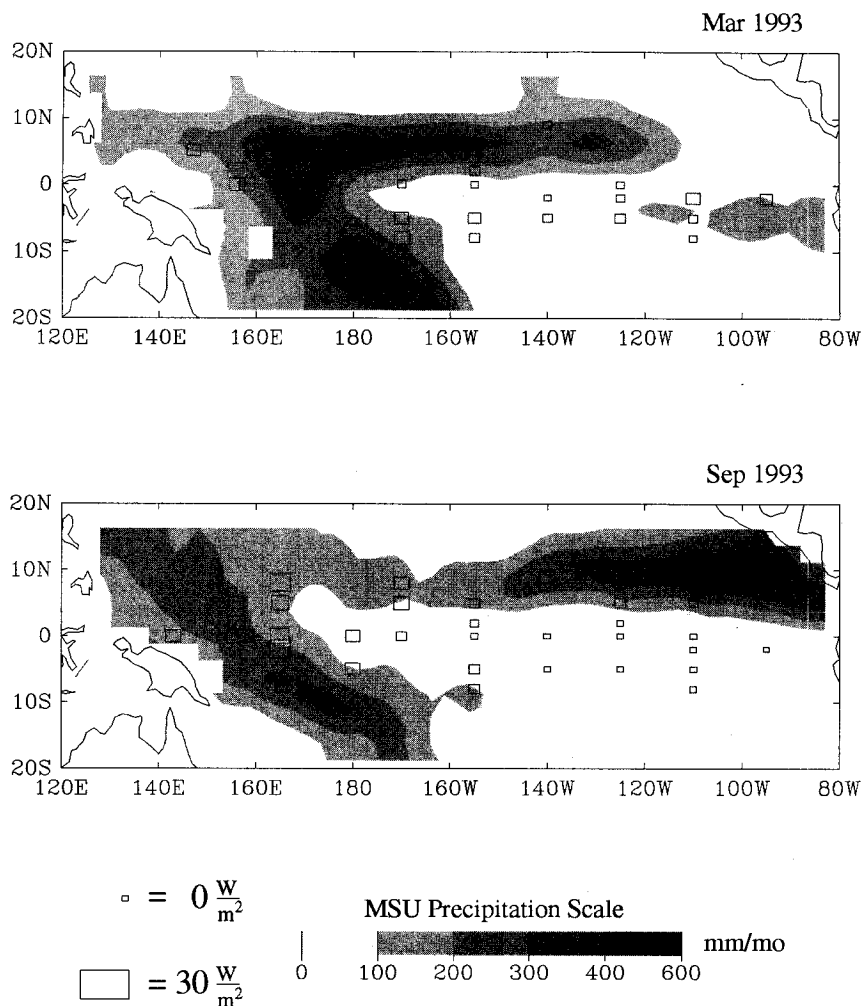## Mesoscale Enhancement of Evaporation

FIG. 6. Comparison of the monthly average mesoscale enhancement of evaporation at TAO mooring locations with MSU estimates of the precipitation pattern over the equatorial Pacific Ocean for (a) March 1993 and (b) September 1993. See section 2b for definition of mesoscale enhancement.

puted, hourly averaged fluxes. Furthermore, the estimates of the daily averaged fluxes computed from the 24 hourly sampled values have very small rms differences and are consistent with the hypothesis that the discrepancies in the hourly estimates are statistically independent and unbiased. Thus, the rms errors introduced by the TAO buoy sampling strategy are not expected to have serious implications for the statistical results of this study. We make an a posteriori check of this assertion in section 4c using data on simultaneous days from the IMET and TAO moorings at 2°S, 156°E during TOGA COARE.

The nominal observation depth for the TAO "sea surface temperature" observation is taken to be 1 m. The nominal observation heights for wind, air temperature, and relative humidity are taken to be $z_u = 3.8$ m, $z_T = z_q = 3$ m, respectively.

For the calculations described below, we will not consider the difference between the near-surface water temperature and the ocean skin temperature at TAO moorings, since incoming radiation instruments are available on only a few of the current generation of moorings. In section 4c, however, we make an estimate of the skin temperature

effects using IMET mooring data from TOGA COARE.

b. TOGA COARE IMET mooring

Processed IMET mooring data, based on observations at 2°S, 156°E during TOGA COARE, were obtained from Dr. Robert Weller at the Woods Hole Oceanographic Institution. In addition to simultaneous measurements of u, v, T, RH, and water temperature with depth, the IMET instrument package measures incoming shortwave and longwave radiation permitting an estimate of ocean skin temperature T_{sfc} using the COARE bulk flux algorithm. The IMET buoy also measures surface currents, so that u and v can be evaluated more accurately as the velocity shear between the wind at z_u and the moving surface, as well as atmospheric pressure and rain rate. The dataset values used in this study are simultaneous 7.5-min averages.

The nominal observation depths for the two IMET subsurface water temperatures used in this study are taken to be 0.45 m and 1 m. The nominal observation heights for wind, air temperature, and relative humidity are taken to be $z_u = 3.4$ m, $z_T = z_q = 2.75$ m, respectively.

c. Monthly averaged precipitation

Monthly averaged large-scale precipitation estimates are used in this study as crude indicators of mesoscale convective system activity in the vicinity of the buoy moorings. One set of estimates was obtained at nominal TOGA TAO and IMET buoy locations from the NOAA GOES Precipitation Index (GPI) archived at the National Center for Atmospheric Research. The GPI is one of the primary tropical precipitation indices used in the global analysis by the Global Precipitation Climatology Project (GPCP). A description of the GPI and the GPCP can be found in Arkin and Xie (1994). To provide a measure of uncertainty in the precipitation estimates, we obtained a second set of independent precipitation estimates based on data from the Microwave Sounding Unit aboard TIROS-N satellites (Spencer 1993). Both datasets were archived as averages over 2.5° lat × 2.5° long grid boxes, which we bilinearly interpolated from the centers of the grid boxes to the buoy locations.

4. Results

a. Mesoscale enhancement in key climatic regimes

To illustrate the influence of precipitating cloud systems on the equatorial Pacific surface fluxes, we present time series from several key climatic regimes sampled by the TOGA TAO buoy array. The major open ocean climatic regimes in the equatorial Pacific are the intertropical convergence zone, stretching from the Central American coast to the western Pacific in the Northern
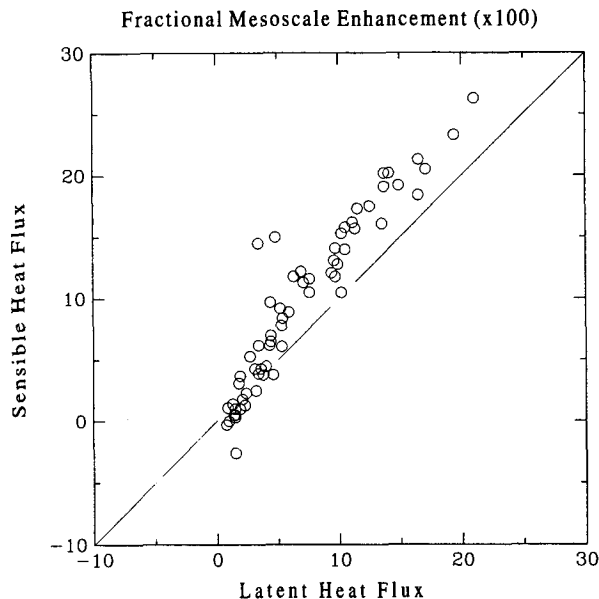
Fractional Mesoscale Enhancement (x100)

FIG. 7. Comparison of fractional mesoscale enhancement of sensible latent heat flux March and September 1993 at TAO moorings with more than 20 days of complete data. The monthly averaged mesoscale enhancements, ΔS and ΔE, are divided by the respective monthly averaged fluxes, $\langle S \rangle$ and $\langle E \rangle$.

Hemisphere; the equatorial cold tongue regime, extending from the South American coast into the central Pacific; the western Pacific warm pool regime; and the easterly trade wind regimes in both the Northern and Southern Hemisphere.

1) TRADE WIND AND ITCZ

The 9°N, 140°W TAO mooring is located in the vicinity of the moving boundary between the North Pacific trade wind regime and the ITCZ. During the Northern Hemisphere winter and spring, relatively strong northeast trade winds dominate conditions at the mooring (Fig. 1a). During the Northern Hemisphere summer and fall, the ITCZ moves into the region of the mooring. The ITCZ conditions coincide with relatively weak winds, high sea surface temperatures, and the largest rainfall rates for the year.

Comparing the daily averaged scalar wind speed $\langle U \rangle$ with the daily averaged vector wind speed V (Fig. 1b), we see that the trade wind regime is relatively steady within the day, while the ITCZ regime has occasionally periods where $(\langle U \rangle - V)/\langle U \rangle$ approaches order one. The magnitude of the monthly averaged air–sea temperature difference and its day-to-day variability are clearly larger in the ITCZ regime during the rainy half of the year from July through December. The air–sea temperature difference is strongly skewed by occasional large negative values, associated with relatively

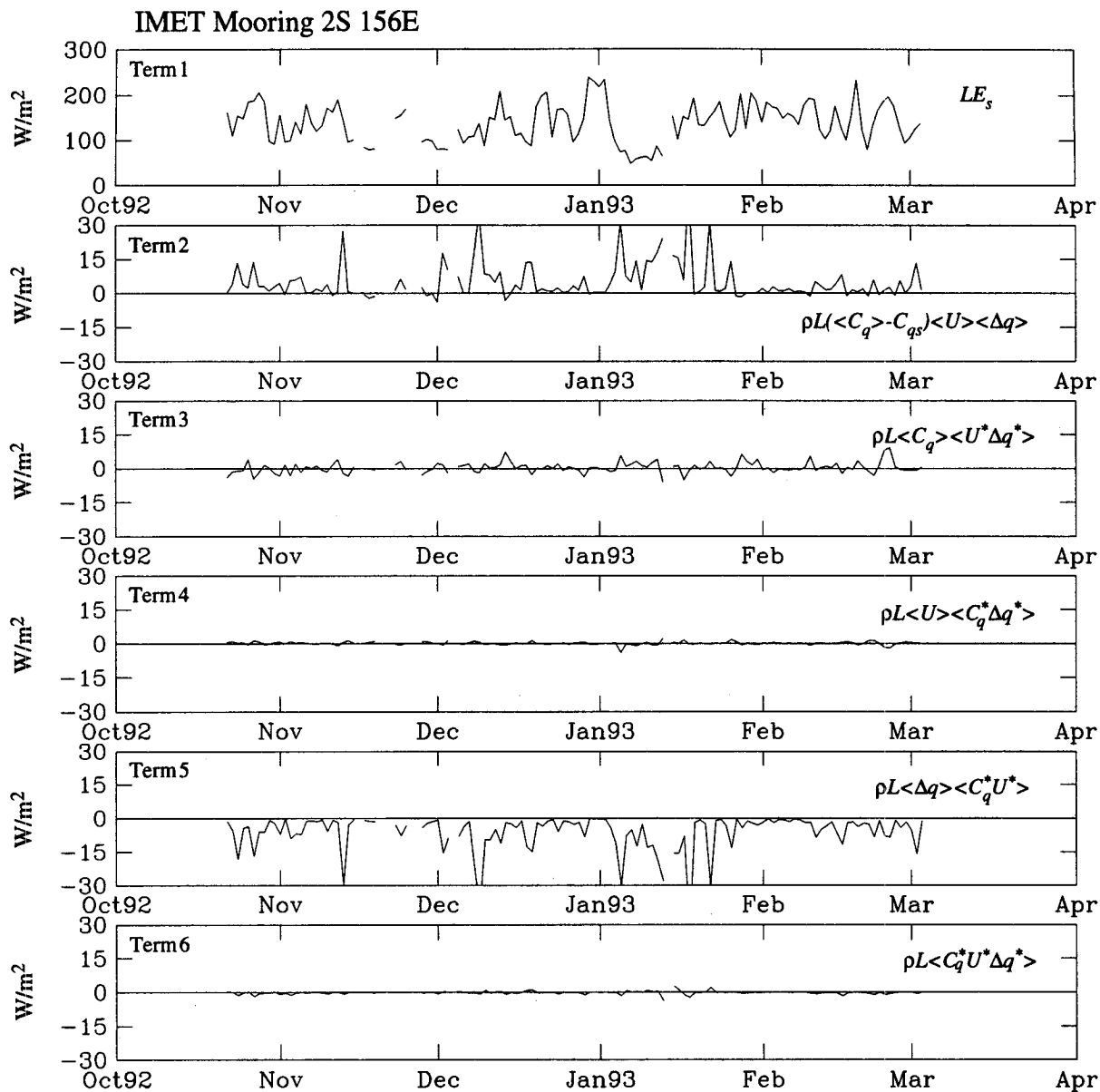## Decomposition of Daily Averaged Latent Heat Flux

FIG. 8. Time series of the Reynolds-averaged decomposition of (a) the daily averaged latent heat flux
and (b) the daily averaged sensible heat flux. See section 4b for details.

cool air temperatures. The magnitude of the air–sea humidity difference increases in the high sea surface temperature regime, but this is not a general feature at all the moorings we have analyzed.

Figures 1c and 1d show that the mesoscale enhancement of evaporation and sensible heat flux is much larger in the ITCZ than in the trade wind regime. Table 3 shows that the statistical distribution of mesoscale enhancement in the ITCZ is strongly skewed by occasional spikes, which are a significant fraction of the total flux. The effects of mesoscale wind variability, that is, $\Delta_v E$ and $\Delta_v S$, are much larger than all remaining effects. The differences between the scalar averaged flux and the total flux for the day, ΔE_s and ΔS_s, are negligible in comparison to $\langle E \rangle$ and $\langle S \rangle$, respectively, as well as $\Delta_v E$ and $\Delta_v S$. In other words, lack of

Decomposition of Daily Averaged Sensible Heat Flux
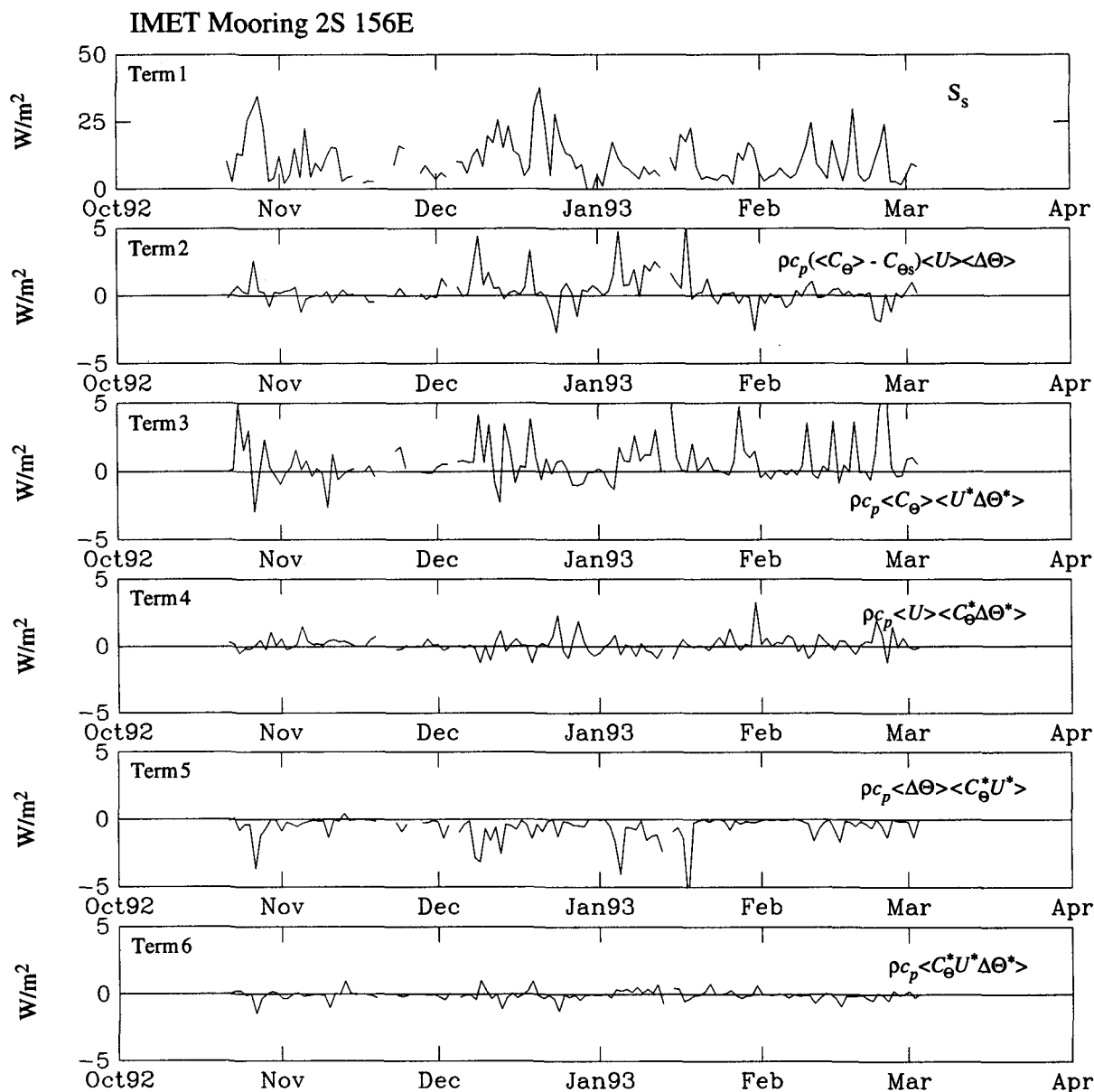
IMET Mooring 2S 156E

FIG. 8. (Continued)

wind steadiness over the period of a day explains nearly all of the mesoscale enhancement of sensible and latent heat fluxes in the ITCZ.

To estimate the magnitude of mesoscale enhancements on monthly averaged surface flux estimates, and to reduce sampling error (sections 2d and 3a), the flux quantities shown in Figs. 1c and 1d are averaged using a 30-day running mean and presented in Fig. 3. The mesoscale enhancements of monthly averaged evaporation and sensible heat flux are

~10% in the ITCZ and are much smaller in the trade wind regime. The enhancements due to mesoscale wind variability are at least an order of magnitude larger than all other effects. The mesoscale enhancement of monthly averaged evaporation fields approaches 30% of the total in the ITCZ during periods when the winds are weak and variable. It is interesting to note that the evaporation changes very little throughout the year despite a large annual cycle in wind speed.

2) WESTERN PACIFIC WARM POOL

The western equatorial Pacific is characterized by relatively weak winds, high sea surface temperatures, and large values of precipitation. In this sense, the meteorological conditions are similar to the ITCZ conditions documented above at the 9°N, 140°W mooring. The mesoscale enhancement statistics at moorings in the western Pacific warm pool region are also similar. As an example, Fig. 4 summarizes mesoscale enhancement estimates at the 2°N, 147°E mooring. Enhancement values are again ~10% of the total evaporation and sensible heat fluxes and are almost entirely explained by lack of wind steadiness. There is an interesting signature of the Madden–Julian oscillation (Madden and Julian 1994) in late 1992 and early 1993 in the time series of evaporation, sensible heat flux and precipitation. During the passage of the waves, there is a mesoscale enhancement of the fluxes due to wind variability. Additional results from the 2°S, 156°E TAO and IMET moorings in the warm pool region are presented in section 4c.

3) COLD TONGUE

The cold tongue region in the eastern equatorial Pacific undergoes a strong annual cycle that is occasionally interrupted by El Niño/Southern Oscillation events (Wallace et al. 1989). The coldest sea surface temperatures typically occur during September and October when the cold tongue extends from the South American coast well out into the central Pacific. Warmest temperatures occur in February through March when the Northern Hemisphere ITCZ nears the equator and a weak ITCZ is often observed in the Southern Hemisphere.

Figure 5 summarizes the mesoscale enhancement estimates for the cold tongue region at the 2°S, 110°W TAO mooring. Mesoscale enhancement is negligibly small throughout the year except during the short period of warm sea surface temperatures and precipitation in the February through April period in each of the three years of record.

4) SPATIAL PATTERN

The relationship between precipitation and mesoscale enhancement of evaporation is again emphasized in the spatial patterns of these quantities for March and September 1993 (Fig. 6). These patterns also reveal subtleties in the relationship not evident in the previous discussion of individual time series. For example, the enhancement values in the region of weak precipitation south of the equator in the central and eastern Pacific during March 1993 are comparable to values obtained in regions of much stronger precipitation in both March and September. It is well known that the structure of an atmospheric mesoscale system is sensitive to the vertical structure of the environmental wind, tempera-

ture, and humidity profiles (e.g., Houze 1993). It is therefore possible that two mesoscale systems may have quite different relationships between the near surface wind and air–sea temperature and humidity differences, and hence differing amounts of enhancement of evaporation and sensible heat flux, even if the amount of precipitation produced by each system over its life cycle is similar.

Figure 7 compares the magnitude of the mesoscale enhancement of sensible and latent heat flux, expressed as a fraction of the respective monthly averaged flux, for March and September 1993 at each TAO mooring location shown in Fig. 6. The mesoscale enhancement is ~10% or less of the total evaporation and sensible heat flux. The sensible heat flux enhancements tend to be larger on a percentage basis than the evaporation enhancements; the slope of a linear fit to 63 data points in Fig. 7 has a 99% confidence interval of [1.14, 1.45]. The largest fractional values of monthly averaged evaporation and sensible heat flux enhancements found at any mooring during these months are 0.21 and 0.26 of the total, respectively. The fractional contributions of $\Delta_s E$ corresponding to the total fractional values shown in Fig. 7 range from -2.0×10^{-2} to 1.4×10^{-2}; in other words the contribution of this effect is almost always smaller than the effect of wind variability, and is two orders of magnitude less than the total evaporation. The corresponding fractional enhancement contributions of $\Delta_s S$ range from -4.4×10^{-2} to 7.9×10^{-2}. In other words, $\Delta_s S$ is occasionally the same magnitude as the contribution of wind variability to the mesoscale enhancement of the sensible heat flux. In nearly all cases, the lack of wind steadiness is the major contributor to the mesoscale enhancement of evaporation and sensible heat flux; the exceptions occur when the mesoscale enhancement values are on the order of a few watts per square meter.

b. Scalar-averaged fluxes

We have found in section 4a that the scalar-averaged latent and sensible heat fluxes for representative TAO moorings and months are within a few percent of the total latent and sensible heat fluxes, respectively. We can also deduce from Figs. 3–7 that the largest values of ΔE and ΔS are generally found in periods with rain and unsteady winds. It is therefore instructive to examine the temporal behavior of the mesoscale enhancement processes in the warm pool region where ΔE and ΔS tend to be largest on a percentage basis.

The small values of ΔE_s and ΔS_s shown in Figs. 1 and 3–5 suggest that the scalar-averaged fluxes E_s and S_s provide very accurate estimates of the total fluxes $\langle E \rangle$ and $\langle S \rangle$, the bulk aerodynamic estimates of the true daily averaged evaporation and sensible flux. This result is consistent with results of recent numerical model simulation by Jabouille et al. (1995) of two convective

cases observed during TOGA COARE. The result is also consistent with the findings of Ledvina et al. (1993) for evaporation estimated over a three-week pre-COARE cruise in the warm pool region, but not for the sensible heat flux. Ledvina et al. (1993) find that the scalar-averaged flux S_s is 60% of the 5 W m^{-2} of total sensible heat flux when averaged over the three-week cruise. The present results from TAO mooring data give a monthly average ΔS_s that is at least an order of magnitude less than the monthly averaged flux in all the major equatorial Pacific climate regimes, including the warm pool region. The reason for the discrepancy is not certain. It may, however, be due to sampling of abnormal or extreme meteorological conditions during the three-week pre-COARE cruise, or due to a combination of instrumental and sampling errors (see section 4c).

To gain insight into the reasons for the accuracy of the scalar-averaged fluxes, the daily averaged bulk aerodynamic flux is decomposed into contributions due to the time mean and perturbation parts of the bulk sea surface temperature and meteorological variables. We write

$$
\begin{array}{cc}
1 & 2 \\
\end{array}
$$
$$
L\langle E\rangle = LE_s + \rho L(\langle C_q\rangle - C_{qs})\langle U\rangle\langle\Delta q\rangle
$$
$$
\begin{array}{cc}
3 & 4 \\
\end{array}
$$
$$
+ \rho L\langle C_q\rangle\langle U^*\Delta q^*\rangle + \rho L\langle U\rangle\langle C_q^*\Delta q^*\rangle
$$
$$
\begin{array}{cc}
5 & 6 \\
\end{array}
$$
$$
+ \rho L\langle\Delta q\rangle\langle C_q^*U^*\rangle + \rho L\langle C_q^*U^*\Delta q^*\rangle \quad (12)
$$
$$
\begin{array}{cc}
1 & 2 \\
\end{array}
$$
$$
\langle S\rangle = S_s + \rho c_p(\langle C_\theta\rangle - C_{\theta s})\langle U\rangle\langle\Delta\theta\rangle
$$
$$
\begin{array}{cc}
3 & 4 \\
\end{array}
$$
$$
+ \rho c_p\langle C_\theta\rangle\langle U^*\Delta\theta^*\rangle + \rho c_p\langle U\rangle\langle C_\theta^*\Delta\theta^*\rangle
$$
$$
\begin{array}{cc}
5 & 6 \\
\end{array}
$$
$$
+ \rho c_p\langle\Delta\theta\rangle\langle C_\theta^*U^*\rangle + \rho c_p\langle C_\theta^*U^*\Delta\theta^*\rangle, \quad (13)
$$

where $C_{qs} \equiv C_q(\langle U\rangle, \langle\cdot\rangle)$, $C_{\theta s} \equiv C_\theta(\langle U\rangle, \langle\cdot\rangle)$, $\Delta q \equiv (\bar{q}_{sfc} - \bar{q})$ and $\Delta\theta \equiv (\bar{\theta}_{sfc} - \bar{\theta})$, Here we have adopted the convention of Ledvina et al. (1993) in breaking out the classical scalar-averaged flux on the rhs of the equations. Overbars denoting a "local average" have been included to avoid ambiguity. The local average is defined over a time period long enough to contain a statistically significant population of the turbulent eddies responsible for surface boundary layer fluxes, but shorter than the characteristic timescale of meso- and synoptic-scale atmospheric systems that constitute the environment of the transporting eddies. Deviations of the locally averaged variables from the larger-scale time means are given by ( )* = ( ) $- \langle( )\rangle$, for example,

$$
\Delta q^* = \bar{q}_{sfc}^* - \bar{q}^* = (\bar{q}_{sfc} - \langle\bar{q}_{sfc}\rangle) - (\bar{q} - \langle\bar{q}\rangle).
$$

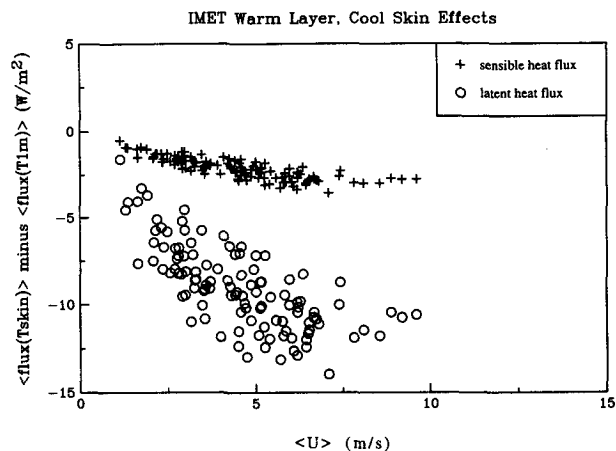IMET Warm Layer, Cool Skin Effects

FIG. 9. Differences in the daily averaged sensible and latent heat fluxes using data from the TOGA COARE IMET mooring, with and without the warm layer, cool skin model in the COARE bulk flux algorithm. The flux estimate assuming T_{sfc} equal to the measured 1-m water temperature is subtracted from the flux that determines T_{sfc} from the warm layer, cool skin model, using the 1-m water temperature as input data.

Figure 8 presents time series of the terms on the rhs of Eqs. (12)–(13) for the TOGA COARE IMET mooring assuming T_{sfc} equals the 0.45-m water temperature. The results show that nonlinearities in the transfer coefficient in the second and fifth terms, and correlations of U with Δq and $\Delta\theta$, are the largest correction terms to E_s and S_s on the rhs of Eqs. (12) and (13), respectively. The fourth term involving correlations of the transfer coefficients with Δq and $\Delta\theta$ and the triple correlation terms are apparently negligible. It is also interesting to note that the discrepancies introduced by the second and fifth term are negatively correlated and tend to cancel each other. This tends to leave $\langle U^*\Delta q^*\rangle$ and $\langle U^*\Delta\theta^*\rangle$ terms as the primary determinants of the sign and magnitude of the discrepancy between the scalar-averaged fluxes and large-scale fluxes.

The results in Fig. 8 depend of course on the choice of transfer coefficient algorithm. With the COARE algorithm, the transfer coefficients tend to decrease with wind speed for constant unstable air–sea temperature and humidity differences. In addition, as wind speed increases, the transfer coefficients tend to decrease rapidly at low wind speeds and less rapidly at higher wind speeds for constant unstable air–sea temperature and humidity differences. There is, thus, a tendency for wind speed to be negatively correlated with the transfer coefficients, and for the mean transfer coefficient to be larger than the value at an intermediate wind speed for constant unstable air–sea temperature and humidity differences. The out of phase relationship between terms 2 and 5 in Fig. 8 are consistent with these tendencies.

TABLE 4a. Mesoscale enhancement statistics at COARE IMET mooring using estimated skin temperature based on the 0.45-m water temperature and observed surface current. See text for details.

Wind (m s^{-1})	Number of days	$L\langle E\rangle$ (W m^{-2})	$\Delta E/\langle E\rangle \times 100$	$\Delta E_s/\langle E\rangle \times 100$	$\langle S\rangle$ (W m^{-2})	$\Delta S/\langle S\rangle \times 100$	$\Delta S_s/\langle S\rangle \times 100$
All	83	115.5	8.7	−0.3	8.0	17.6	6.5
≤4	34	83.8	14.2	−0.7	5.7	26.0	8.2
>4	49	137.5	6.3	−0.1	9.5	14.4	5.8

c. Skin temperature, spatial sampling, and surface current effects

In this section, we investigate several sources of error in mesoscale enhancement calculations by taking advantage of the colocation of the TAO and IMET moorings at 2°S, 156°E during TOGA COARE. In particular, we examine the error caused by neglecting the warm layer, cool skin effects, and surface currents in the bulk aerodynamic computations at TAO moorings, as well as sampling errors due to the nominal spatial separation of approximately 25 km between the TAO and IMET moorings.

As mentioned previously, the mesoscale enhancement estimates reported in section 4a are calculated with the ocean skin temperature T_{sfc} set equal to the TAO mooring 1-m water temperature. The "warm layer, cool skin" model included in the COARE algorithm was not used. Warm layer effects are expected to be largest when wind speeds are less than 4 m s^{-1} and the solar radiation is large (e.g., Fairall et al. 1996a). These conditions were obtained during several periods in the warm pool region sampled by the IMET mooring.

Figure 9 shows the difference between the daily averaged evaporation and sensible heat flux with and without a proper accounting for warm layer, cool skin effects at the IMET mooring. The flux was first calculated using the COARE algorithm without the warm layer, cool skin option; the flux was then calculated in an identical manner except for the inclusion of the warm layer, cool skin option. The subsurface water temperature at 1 m was used as the water temperature input for both calculations. Since the TAO mooring water temperature nearest the surface is at 1-m depth, the difference presented here is an estimate of the error due to neglect of warm layer, cool skin effects in the TAO flux estimates presented in this study.

At wind speeds greater than 4 m s^{-1}, Fig. 9 suggests that the cool skin effect dominates the statistics for the

day, resulting in lower daily averaged evaporation and sensible heat fluxes. At low wind speeds, the warm layer effect compensates for the effect of the cool skin in the average for the day. The average reductions of the sensible and latent heat fluxes for the entire COARE period are 2.1 W m^{-2} and 9.0 W m^{-2}, respectively. For very light winds ($\sim$1 m s^{-1}) and relatively clear sky conditions, we might expect the sign of the daily averaged warm layer, cool skin effects to become positive, but our dataset did not contain enough days of very light winds to provide a statistically significant estimate of this effect.

Statistics related to the mesoscale enhancement of the daily averaged total fluxes at the 2°S, 156°E IMET and TAO moorings are shown in Table 4. IMET mooring results are shown with and without warm layer, cool skin effects. We have used only those days for which we were able to calculate fluxes continuously for the 24-h period at both the TAO and IMET moorings. The arithmetic average of the two daily averaged wind speed values was used to stratify the flux statistics. The fractional values are computed from the ratio of the mean values for each wind speed category.

From Table 4, we see that the warm layer, cool skin physics included in the COARE flux algorithm and the inclusion of surface current effects make quantitative differences in the values of the flux and mesoscale enhancement statistics for both the low and moderate wind speed regimes. Qualitatively, however, the conclusions that one would draw regarding the mesoscale enhancement statistics for the IMET mooring would be the same whether the warm layer, cool skin or current effects are included or not.

Over the 83 days of common record, the average mesoscale enhancement at the IMET mooring is $\sim$10% of the total flux, and, in light wind speed conditions, the average mesoscale enhancements reach maxima of approximately 15% and 25% of the total evaporation and sensible heat flux, respectively. This is consistent

TABLE 4b. COARE IMET mooring using estimated skin temperature based on the 0.45-m water temperature and assuming zero surface current.

Wind (m s^{-1})	Number of days	$L\langle E\rangle$ (W m^{-2})	$\Delta E/\langle E\rangle \times 100$	$\Delta E_s/\langle E\rangle \times 100$	$\langle S\rangle$ (W m^{-2})	$\Delta S/\langle S\rangle \times 100$	$\Delta S_s/\langle S\rangle \times 100$
All	83	117.8	8.3	−0.3	8.1	17.0	6.3
≤4	34	84.9	13.9	−0.6	5.8	25.0	8.3
>4	49	140.6	6.0	−0.1	9.7	13.8	5.5

TABLE 4c. COARE IMET mooring using 1-m subsurface water temperature and assuming zero surface current.

Wind (m s^{-1})	Number of days	$L\langle E\rangle$ (W m^{-2})	$\Delta E/\langle E\rangle \times 100$	$\Delta E_s/\langle E\rangle \times 100$	$\langle S\rangle$ (W m^{-2})	$\Delta S/\langle S\rangle \times 100$	$\Delta S_s/\langle S\rangle \times 100$
All	83	126.4	8.2	−0.2	10.2	15.5	5.5
≤4	34	91.6	13.8	−0.3	7.3	24.1	8.5
>4	49	150.5	5.8	−0.2	12.2	12.0	4.2

with our findings using all of the TAO mooring data. There is a qualitative difference, however, in the fraction of the mesoscale enhancement that is explained by lack of wind steadiness. The IMET mooring data suggests that a greater fraction of the mesoscale enhancement is explained by other processes, such as the correlation of stronger winds with larger air–sea temperature and humidity differences. This might explain some of the discrepancy between the scalar-averaged sensible heat flux results reported in this study and the results reported by Ledvina et al. (1993) for the three-week pre-COARE cruise in light winds over the warm pool. The differences between TAO and IMET estimates are most notable for sensible heat flux and less for latent heat flux.

Comparing the TAO and IMET mooring results in Table 4, we see that the total estimated fluxes are in very close quantitative and qualitative agreement for all wind speed regimes. The rms differences between simultaneous daily sensible and latent heat flux values at the two buoys are 8 W m^{-2} and 40 W m^{-2}, respectively. Some of these differences may be due to the 25 km spatial separation of the buoys. Nevertheless, while the difference in the daily simultaneous fluxes can be large, averaged over the entire TOGA COARE period they are small (on the order of one standard error, assuming the differences are uncorrelated normal random noise). This suggests that the temporal and spatial sampling errors discussed in sections 2d and 3a are not important for the conclusions of this study.

5. Conclusions and discussion

On the basis of surface marine meteorological data from TOGA TAO moorings and the TOGA COARE bulk aerodynamic flux algorithm, the magnitude of the mesoscale enhancement of monthly averaged sea surface evaporation is estimated to be ∼10% or less of the total evaporation over the equatorial Pacific Ocean. During occasional periods with weak and variable winds over the western Pacific warm pool and the other

major precipitation zones in the equatorial Pacific, the mesoscale enhancement of monthly averaged evaporation fields can reach 30% of the total evaporation. The mesoscale enhancement was found to be due primarily to the lack of wind steadiness.

The magnitude of the sensible heat flux enhancement by mesoscale systems is found to be similar to the evaporation enhancement, but we are less certain about the primary importance of mesoscale wind variability in the case of the sensible heat flux. A recent numerical model simulation by Jabouille et al. (1995) of two convective cases observed during TOGA COARE supports the conclusion that mesoscale wind variability plays a major role in determining the mesoscale enhancement of both the sensible and latent heat fluxes. The model integration assumed that the sea surface temperature is a constant, however, and it is not obvious how the model results would change when the sea surface temperature assumption is relaxed. Furthermore, our comparison of results from colocated TOGA TAO and IMET moorings, and the previously reported results of Ledvina et al. (1993), indicate that the contribution of processes other than wind variability may be equally important for the enhancement of the sensible heat flux.

The reader should note that the conclusion regarding the importance of mesoscale wind variability does not imply that thermodynamic effects of mesoscale systems can be ignored in parameterizations for large-scale numerical or theoretical models. The large-scale air–sea humidity and temperature differences are determined in part by the vertical exchange of heat, moisture, and momentum between the boundary layer and the free atmosphere, including the net effect of mesoscale convective system components such as convective and mesoscale downdrafts and updrafts. Rather, the conclusion regarding wind variability simply focusses attention on the need to determine all-weather mesoscale surface wind speed statistics to achieve an accuracy of 10 W m^{-2} for evaporative heat flux estimates on timescales of a season or longer when using the bulk aerodynamic formulas.

TABLE 4d. The 2°S,156°E TAO mooring.

Wind (m s^{-1})	Number of days	$L\langle E\rangle$ (W m^{-2})	$\Delta E/\langle E\rangle \times 100$	$\Delta E_s/\langle E\rangle \times 100$	$\langle S\rangle$ (W m^{-2})	$\Delta S/\langle S\rangle \times 100$	$\Delta S_s/\langle S\rangle \times 100$
All	83	120.8	8.4	−0.8	9.0	11.6	1.9
≤4	34	86.1	17.1	−1.2	6.3	22.7	3.3
>4	49	144.9	4.8	−0.6	10.8	7.0	1.3

We now return to the question of whether existing climatologies have missed a large contribution of atmospheric mesoscale systems to tropical surface evaporation and sensible heat flux. On the basis of our study, the contributions of atmospheric mesoscale systems to the total evaporative and sensible heat fluxes appear to be in the range of 0%–30%. Previous studies have indicated that the classical method of using monthly averaged wind speed and thermodynamic data may be used to calculate monthly average evaporation and sensible heat flux to within a relative error of ~10% (see introduction); Zhang (1995) has confirmed this result for the equatorial Pacific using TOGA TAO buoy data. We therefore suggest that most of the enhancement of tropical ocean evaporation and sensible heat flux by atmospheric mesoscale systems is represented in existing climatologies. The discrepancies between the existing climatological fields are more likely to be due to differences in bulk parameterizations, the time period of the data, instrumental error, and undersampling in data sparse regions of the Tropics, than on whether the classical or sampling methods are employed. In any case, the mesoscale contributions to the total heat flux are the same order as the errors typically quoted for uncertainties in bulk aerodynamic transfer coefficients and systematic data errors (e.g., Weare 1989).

Recent improvements in bulk aerodynamic formulas (e.g., Fairall et al. 1996) and historical datasets (e.g., DaSilva et al. 1994) will ultimately lead to quantitative improvement in climatological evaporation and sensible heat flux estimates in data dense regions. Large sampling errors will still be possible, however, in convectively active, data sparse regions, where the statistical distribution of mesoscale enhancements and the air–sea temperature differences may be strongly skewed (see section 4a.1). Quantitative estimates of such sampling errors could be obtained from an observing system simulation experiment using long data records from TOGA TAO moorings.

REFERENCES

Arkin, P. A., and P. Xie, 1994: The Global Precipitation Climatology Project: First algorithm intercomparison project. *Bull. Amer. Meteor. Soc.*, **75**, 401–419.
Buck, A. L., 1981: New equations for computing vapor pressure and enhancement factor. *J. Appl. Meteor.*, **20**, 1527–1532.
Budyko, M. I., Ed., 1963: *Atlas of the Heat Balance of the Earth* (in Russian). Akad. Nauk SSSR, Prezidium, Mezhduvedomstvennyi Geofiz. Komitet., 69 pp. [Published in English as *Guide to the Atlas of the Heat Balance of the Earth,* translated by I. A. Donehoo, U.S. Weather Bureau, WB/T-106, Washington, DC.]
Businger, J. A., 1982: The fluxes of specific enthalpy, sensible heat and latent heat near the earth's surface. *J. Atmos. Sci.*, **39**, 1889–1892.
DaSilva, A. M., C. C. Young, and S. Levitus, 1994: *Atlas of Surface Marine Data 1994,* National Oceanic and Atmospheric Administration, XXX pp.
Esbensen, S. K., and Y. Kushnir, 1981: The heat budget of the global ocean: An atlas based on estimates from surface marine observations. Climatic Research Institute Rep. No. 29, Oregon State University, Corvallis, OR, 27 pp. + plates. [Available from College of Oceanic and Atmospheric Sciences, Oregon State University, Corvallis, OR 97331-2209.]
——, and R. W. Reynolds, 1981: Estimating monthly averaged air–sea transfers of heat and momentum using the bulk aerodynamic method. *J. Phys. Oceanogr.*, **11**, 457–465.
Fairall, C. W., E. F. Bradley, J. S. Godfrey, G. A. Wick, J. B. Edson, and G. S. Young, 1996a: Cool-skin and warm-layer effects on sea surface temperature. *J. Geophys. Res.*, **101**(C1), 1295–1308.
——, ——, D. P. Rogers, J. B. Edson, and G. S. Young, 1996b: Bulk parameterization of air–sea fluxes for TOGA COARE. *J. Geophys. Res.*, **101**, 3747–3764.
Gulev, S. K., 1994: Influence of space–time averaging on the ocean–atmosphere exchange estimates in the North Atlantic midlatitudes. *J. Phys. Oceanogr.*, **24**, 1236–1255.
Hayes, S. P., L. J. Mangum, J. Picaut, A. Sumi, and K. Takeuchi, 1991: TOGA-TAO: A moored array for real-time measurements in the tropical Pacific Ocean. *Bull. Amer. Meteor. Soc.*, **72**, 339–347.
Houze, R. A., 1993: *Cloud Dynamics.* Academic Press, 573 pp.
Hsuing, J., 1986: Mean surface energy fluxes over the global ocean. *J. Geophys. Res.*, **91**, 10 585–10 606.
Jabouille, P., J. L. Redelsperger, and J. P. Lafore, 1996: Modification of surface fluxes by atmospheric convection in the TOGA COARE region. *Mon. Wea. Rev.*, **124**, 816–837.
Johnson, R. H., and M. E. Nicholls, 1983: A composite analysis of the boundary layer accompanying a tropical squall line. *Mon. Wea. Rev.*, **111**, 308–319.
Josey, S. A., E. C. Kent, and P. K. Taylor, 1995: Seasonal variations between sampling and classical mean turbulent heat flux estimates in the eastern North Atlantic. *Ann. Geophys.*, **13**, 1054–1064.
Kent, E. C., P. K. Taylor, B. S. Truscott, and J. S. Hopkins, 1993: The accuracy of voluntary observing ships' meteorological observations—Records of the VSOP-NA. *J. Atmos. Oceanic Technol.*, **10**, 591–608.
Ledvina, D. V., G. S. Young, R. A. Miller, and C. W. Fairall, 1993: The effect of averaging on bulk estimates of heat and momentum fluxes for the tropical western Pacific Ocean. *J. Geophys. Res.*, **98**, 20 211–20 217.

Liu, W. T., 1988: Moisture and latent heat flux variabilities in the tropical Pacific derived from satellite data. *J. Geophys. Res.,* **93**(C6), 6749–6760.

——, K. B. Katsaros, and J. A. Businger, 1979: Bulk parameterization of air–sea exchanges of heat and water vapor including molecular constraints at the interface. *J. Atmos. Sci.,* **36,** 1722–1735.

Madden, R. A., and P. R. Julian, 1994: Observations of the 40–50-day tropical oscillation—A review. *Mon. Wea. Rev.,* **122,** 814–837.

Mahrt, L., and J. Sun, 1995: Dependence of surface exchange coefficients on averaging scale and grid size. *Quart. J. Roy. Meteor. Soc.,* **121,** 1835–1852.

——, C. Berthou, P. Marquet, and J. C. Andre, 1986: Time-averaging the flux profile relationship. *Ann. Geophys.,* **4,** 411–416.

McPhaden, M. J., 1995: The Tropical Atmosphere Ocean array is completed. *Bull. Amer. Meteor. Soc.,* **76,** 739–741.

Miller, M. J., A. C. M. Beljaars, and T. N. Palmer, 1992: The sensitivity of the ECMWF model to the parameterization of evaporation from tropical oceans. *J. Climate,* **5,** 418–434.

Oberhuber, J. M., 1988: An atlas based on the "COADS" data set: The budgets of heat, buoyancy and turbulent kinetic energy at the surface of the global ocean. Max-Planck-Institut für Meteorologie Rep. No. 15, Hamburg, 20 pp. + plates. [Available from Max-Planck-Institut für Meteorollgie, Bündesstrasse 55, D-2000 Hamburg 13, Germany.]

Spencer, R. W., 1993: Global oceanic precipitation from MSU during 1979–91 and comparisons to other climatologies. *J. Climate,* **6,** 1301–1326.

Sun, J., and L. Mahrt, 1995: Determination of surface fluxes from the surface radiative temperature. *J. Atmos. Sci.,* **52,** 1095–1106.

——, S. K. Esbensen, and L. Mahrt, 1995: Estimation of surface heat flux. *J. Atmos. Sci.,* **52,** 3162–3171.

——, L. Mahrt, S. K. Esbensen, J. Howell, C. M. Greb, R. Grossman, and M. A. LeMone, 1996: Scale dependence of air–sea fluxes over the western equatorial Pacific. *J. Atmos. Sci.,* **53,** 2997–3012.

Wallace, J. M., T. P. Mitchell, and C. Deser, 1989: The influence of sea-surface temperature on surface wind in the eastern equatorial Pacific: Seasonal and interannual variability. *J. Climate,* **2,** 1492–1499.

Weare, B. C., 1989: Uncertainties in estimates of surface heat fluxes derived from marine reports over the tropical and subtropical oceans. *Tellus,* **41,** 357–370.

Young, G. S., D. V. Ledvina, and C. W. Fairall, 1992: Influence of precipitating convection on the surface energy budget observed during a Tropical Ocean Global Atmosphere pilot cruise in the tropical western Pacific Ocean. *J. Geophys. Res.,* **97,** 9595–9603.

Zhang, G. J., 1995: On the use of monthly mean data to compute surface turbulent fluxes in the tropical Pacific. *J. Climate,* **8,** 3084–3090.